

First Detection of Molecular Gas in the Giant Low Surface Brightness Galaxy Malin 1

GASPAR GALAZ,¹ JORGE GONZÁLEZ-LÓPEZ,^{1,2} VIVIANA GUZMÁN,¹ HUGO MESSIAS,³ JUNAIS,^{4,5} SAMUEL BOISSIER,⁶ BENOÎT EPINAT,^{7,6} PETER M. WEILBACHER,⁸ THOMAS PUZIA,¹ EVELYN J. JOHNSTON,⁹ PHILIPPE AMRAM,⁶ DAVID FRAZER,¹⁰ MATÍAS BLAÑA,¹¹ J. CHRISTOPHER HOWK,¹² MICHELLE BERG,¹³ ROY BUSTOS-ESPINOZA,¹ JUAN CARLOS MUÑOZ-MATEOS,¹⁴ PAULO CORTÉS,^{15,16} DIEGO GARCÍA-APPADOO,¹⁷ AND KATERINE JOACHIMI¹⁸

¹*Instituto de Astrofísica, Pontificia Universidad Católica de Chile, Vicuña Mackenna 4860, Macul, Santiago, Chile*

²*Las Campanas Observatory, Carnegie Institution for Science, Raúl Bitrán 1200, La Serena, Chile*

³*Joint ALMA Observatory, Alonso de Córdova 3107, Vitacura 763-0355, Santiago, Chile*

⁴*Instituto de Astrofísica de Canarias, Vía Láctea S/N, E-38205 La Laguna, Spain*

⁵*Departamento de Astrofísica, Universidad de La Laguna, E-38206 La Laguna, Spain*

⁶*Aix-Marseille Univ, CNRS, CNES, LAM (Laboratoire d'Astrophysique de Marseille), Marseille, France*

⁷*Canada-France-Hawaii Telescope, 65-1238 Mamalahoa Highway, Kamuela, HI 96743, USA*

⁸*Leibniz-Institut für Astrophysik Potsdam (AIP), An der Sternwarte 16, 14482 Potsdam, Germany*

⁹*Instituto de Estudios Astrofísicos, Facultad de Ingeniería y Ciencias, Universidad Diego Portales, Av. Ejército Libertador 441, Santiago, Chile*

¹⁰*Green Bank Observatory, PO Box 2, Green Bank, WV, 24944, USA*

¹¹*Instituto de Alta Investigación, Universidad de Tarapacá, Casilla-7D, Arica, Chile*

¹²*Department of Physics and Astronomy, University of Notre Dame, Notre Dame, IN 46556, USA*

¹³*Department of Astronomy, The University of Texas at Austin, Austin, TX 78712, USA*

¹⁴*European Southern Observatory, Karl-Schwarzschild Straße 2, 85748 Garching bei München, Germany*

¹⁵*Joint ALMA Observatory, Alonso de Córdoba 3107, Vitacura, Santiago, Chile*

¹⁶*National Radio Astronomy Observatory, 520 Edgemont Road, Charlottesville, VA 22903, USA*

¹⁷*Esinel Ingenieros, Holanda 100, Providencia, Santiago, Chile*

¹⁸*Universidad Técnica Federico Santa María, Vicuña Mackenna 3939, San Joaquín, Santiago, Chile*

(Received 2024 September 20; Revised 2024 October 9; Accepted 2024 October 12)

ABSTRACT

After over three decades of unsuccessful attempts, we report the first detection of molecular gas emission in Malin 1, the largest spiral galaxy observed to date, and one of the most iconic giant low surface brightness galaxies. Using ALMA, we detect significant $^{12}\text{CO}(\text{J}=1-0)$ emission in the galaxy's central region and tentatively identify CO emission across three regions on the disc. These observations allow for a better estimate of the H_2 mass and molecular gas mass surface density, both of which are remarkably low given the galaxy's scale. By integrating data on its HI mass, we derive a very low molecular-to-atomic gas mass ratio. Overall, our results highlight the minimal presence of molecular gas in Malin 1, contrasting sharply with its extensive, homogeneous atomic gas reservoir. For the first time, we position Malin 1 on the Kennicutt-Schmidt (K-S) diagram, where it falls below the main sequence for normal spirals, consistent with previous upper limits but now with more accurate figures. These findings are crucial for constraining our understanding of star formation processes in environments characterized by extremely low molecular gas densities and for refining models of galaxy formation, thereby improving predictions concerning the formation, evolution, and distribution of these giant, elusive galaxies.

Keywords: Spiral galaxies (1560); Spiral arms (1559); Molecular gas (1073); Low surface brightness galaxies (940); Detection (1911); Diffuse molecular clouds (381); Interferometers (805)

1. INTRODUCTION

Low surface brightness galaxies (LSBGs) exhibit surface brightness (SB) levels that are fainter than the dark night sky (Disney 1976). Current data indicate that they dominate the galaxy volume number density (Dalcanton et al. 1997; O’Neil & Bothun 2000; Martin et al. 2019).

Being quite difficult to detect in typical magnitude limited optical surveys (de Blok & McGaugh 1997), LSBGs are characterized by low stellar and star formation densities (van der Hulst et al. 1993; Gerritsen & de Blok 1999), and their neutral hydrogen dominance makes molecular gas tracers particularly elusive (Pickering et al. 1997; O’Neil et al. 2000, 2023).

The existence of a large population of low surface brightness galaxies (LSBGs) appeared in the debate in the seventies when, at first glance, observations from photographic plates suggested a faintest surface brightness for discs in spiral galaxies, an idea which converged in those years to the so-called “Freeman’s law” (Freeman 1970). The fact that this was proved afterwards to be a bias introduced by photographic plates themselves (Disney 1976) triggered the search of LSBGs both in already available photographic plates as well as in new surveys (Maddox et al. 1990; Impey et al. 1996). It was in this way that the giant low surface brightness galaxy (gLSBG) Malin 1 was accidentally discovered, when astronomers were searching for LSBGs from photographic plates in the eighties. Initially, it appeared as a normal spiral galaxy, surrounded by a barely visible nebulosity (Bothun et al. 1987). Subsequent HI observations revealed that the galaxy possesses an enormous HI disc, with an extent of several arcmin in the sky (Bothun et al. 1987). However, the shocking aspect was not only the diffuse structure barely observed in the optical, but the physical size of Malin 1. The redshift measured both in the optical and in HI ($z \sim 0.082$) indicated that Malin 1 has a diameter *at least* of hundreds of kiloparsecs ($\sim 100-150$ kpc up to a photographic isophote reaching 25 mag arcsec^{-2} , measured at those years).

This discovery immediately placed Malin 1 as one of the largest disc galaxies, with one of the most massive HI reservoirs ($M_{\text{HI}} \sim 4-7 \times 10^{10} M_{\odot}$) (Impey & Bothun 1989; Pickering et al. 1997; Lelli et al. 2010), and exhibiting one of the faintest discs ever observed in the optical, with a central surface brightness (SB) of ~ 25.5 mag arcsec^{-2} in the V band (Impey & Bothun 1989). A detailed spectroscopic analysis also hinted for the presence

of an active galactic nucleus (AGN) in the central part of Malin 1. Initially classified as a Seyfert 1 (Impey & Bothun 1989), it was later reclassified as a low-ionization nuclear emission-line region AGN type (LINER) (Barth 2007).

Spectroscopic studies of Malin 1 revealed nebular emission lines, indicating likely stellar formation. Barth (2007) detected $\text{H}\alpha$ and other emission lines from the nucleus but did not explore stellar formation. Junais et al. (2020) also found nebular emission lines from the central regions with the VLT. SFRs derived from $\text{H}\alpha$ fluxes suggest an early-type disk in the inner region and extended UV-like galaxies in the outer parts. They also noted high metallicity and low dust content in the inner regions.

Boissier et al. (2016) conducted a multi-band photometric study, showing that the surface brightness and color profiles suggest a long, quiet star-formation history, with angular momentum 20 times that of the Milky Way. They found an SFR of $\sim 2 M_{\odot} \text{ yr}^{-1}$ and concluded that the star formation scenario did not require galaxy interactions.

Regarding the environment, Malin 1 interacts with two compact galaxies, Malin 1A and Malin 1B (Reshetnikov et al. 2010; Galaz et al. 2015; Saha et al. 2021), and possibly a galaxy 350 kpc away (Reshetnikov et al. 2010; Galaz et al. 2015). Otherwise, it is relatively isolated within 1 Mpc (Bustos-Espinoza et al. 2025, in preparation).

Finally, Junais et al. (2024) used VLT/MUSE to detect nebular emission lines in the disk, confirming recent star formation in several regions, as earlier suspected by other authors (Bothun et al. 1987). This work will be referenced throughout this paper.

Current figures suggest that Malin 1 is perhaps the largest known spiral galaxy, with a disc diameter of ~ 200 kpc and a SB fainter than 28.0 mag arcsec^{-2} in the optical B band, with very diffuse but thick and rich spiral arms (Galaz et al. 2015; Boissier et al. 2016; Saha et al. 2021).

The features described above settled the scenario for discovering the presence of molecular gas in Malin 1, which was intensively searched shortly after its discovery. However, these searches and all posterior ones, during the last 30 years, failed (Impey & Bothun 1989; Radford 1992; Braine et al. 2000; Galaz et al. 2022). In summary, these figures set a quite perplexing picture: the

largest spiral galaxy discovered so far, without a trace of molecular gas over its ~ 200 kpc diameter.

Here, we report the first measurement of molecular gas emission in Malin 1. Using ALMA band 3 and the most compact array configuration, observations in the first semester of 2024 reveals the presence of continuum emission and $^{12}\text{CO}(1-0)$ line emission, with significant flux in the central part and tentative emission in three other regions in the disc.

We present observations in §2, data analysis and some direct results in §3. In §4 we present some physical estimates and discussion, and we summarize and conclude in §5. Throughout this paper we assume a ΛCDM cosmology with parameters $H_0 = 70 \text{ km s}^{-1} \text{ Mpc}^{-1}$, $\Omega_M = 0.3$, and $\Omega_\Lambda = 0.7$, and a heliocentric redshift for Malin 1 of $z = 0.082702$. With these parameters, Malin 1 has a distance of 370 Mpc and a plate scale of $1.57 \text{ kpc arcsec}^{-1}$.

2. OBSERVATIONS

ALMA band 3 observations were carried on during March 2024, using the most compact configuration C-1 of the 12m array. The total on-source time was 5.64 hrs splitted in two pointings separated by 39 arcsec. The first pointing was centered in the bulge of the galaxy (J2000: RA 12:36:59, DEC +14:19:49), and the second one in a disc region located to the North West (J2000: RA 12:36:57, DEC +14:20:15). The choice of this last region was motivated by recent VLT/MUSE results, showing bright emission from this place (Junais et al. 2024). Considering the rest frequency of 115.271202 GHz for the $^{12}\text{CO}(1-0)$ line, and given the heliocentric redshift of Malin 1, the observed frequency for $^{12}\text{CO}(1-0)$ was tuned to 106.458562 GHz. The continuum was observed in four spectral windows, each with 1875 MHz bandwidth.

Observations were calibrated using CASA¹ version 6.5.4.9 and the ALMA pipeline version 2023.1.0.124. The imaging of the observations returns a natural weighting synthesized beam of $3.76 \text{ arcsec} \times 3.41 \text{ arcsec}$ and a position angle of -63.9 deg for the continuum image. Similar synthesized beams are obtained for the spectral cubes created for the individual spectral windows.

The first step in imaging the data was to create a multi-frequency synthesis (MFS) of all available spectral windows and channels, and all the pointings using the mosaic option as a gridded. All images and cubes were cleaned using the auto-masking option known as “auto-

multithresh”. Cleaning masks were created over all the features above 4σ significance level, where σ value is calculated automatically by CLEAN in the residuals using a robust rms estimate. Masks were expanded down to 2σ and cleaned down to 1σ .

3. DATA ANALYSIS AND RESULTS

3.1. *Detections*

The final image combines the continuum and potential line emission. We are clearly detecting a source in the galaxy’s bulge with a signal-to-noise ratio above 17.

Left panel of Figure 1, shows the $^{12}\text{CO}(1-0)$ line detection contours in the central part, super-imposed on a composite optical image of Malin 1 from Boissier et al. (2016). We also show the boundaries of the region covered by our ALMA observations by a segmented line. Specifically, the line indicates where the Primary Beam (PB) correction reaches 0.3 (i.e., a depth of 30% relative to that reached at the phase center). The right panels show the continuum and line contours super-imposed on the $\text{H}\alpha$ emission obtained recently with MUSE at the VLT by Junais et al. (2024). It is worth noting the double emission feature of the $\text{H}\alpha$ emission in the central part. This has been discussed as a possible double central star cluster (Johnston et al. 2024), where significant $\text{H}\alpha$ emission is being emitted. The southern $^{12}\text{CO}(1-0)$ emission in the central part coincides with the $\text{H}\alpha$ emission shown by Johnston et al. (2024), and contours at different significance levels clearly show that the detection is statistically significant at $\simeq 6\sigma$ (see Figure 1). It is apparent that the continuum seems better aligned with $\text{H}\alpha$ than the CO. This could be because of the higher S/N, giving us a better precision and the offset seen in $^{12}\text{CO}(1-0)$ is just produced by low S/N. Also, the offset between the centroids of $\text{H}\alpha$ and $^{12}\text{CO}(1-0)$ are well within the typically accepted centroid precision of ALMA observations of around 0.1-0.2 times the beam size (~ 4.5 arcsec), i.e., 0.45-0.90 arcsec.

We detect an emission line associated with the nucleus with a significance of $\text{S/N} = 6.5$ centered at 106.518 GHz. Figure 2 shows the $^{12}\text{CO}(1-0)$ line profile, fitted to the ALMA band 3 data for the central region described in Figure 1. It provides the flux intensity as a function of the velocity offset with respect to the optical redshift of the galaxy.

The measured deviation of -120 km s^{-1} of the central CO emission observed in Figure 2 with the systemic velocity², compared to the corresponding $\sim -20 \text{ km s}^{-1}$ from MUSE stellar and ionized gas kinematics (John-

¹ CASA, Common Astronomy Software Application, provided by ALMA Observatory.

² Obtained with the heliocentric redshift used in this study.

ston et al. 2024), is compatible with the large velocity dispersion of $\sim \pm 200 \text{ km s}^{-1}$ measured with MUSE in the central regions from both ionized gas and stars. The small offset of the CO center to the south-west with respect to the ionized gas and stellar distributions may also induce lower velocities. The relatively large velocity width in CO at the center is an additional hint which supports that this central CO detection belongs to Malin 1.

For the central part, the flux density for the continuum is $107 \pm 12 \mu\text{Jy}$ and the velocity-integrated flux density for the $^{12}\text{CO}(1-0)$ line is $143 \pm 41 \text{ mJy km s}^{-1}$.

To measure the integrated flux and angular extension of the emission lines we proceeded to do a continuum subtraction both in the image plane and in the uv-plane. We used IMCONTSUB from the CASA package to subtract the continuum emission fitted in the range of frequencies surrounding the detected line. After the continuum subtraction, a moment-0 was created collapsing the channels with emission associated with the central line. The line emission was then fitted using IMFIT within CASA (and returned the integrated flux of $143 \pm 41 \text{ mJy km s}^{-1}$ mentioned before). The line is also barely resolved with a FWHM major axis of $4.4 \pm 1.9 \text{ arcsec}$, a minor axis of $2.6 \pm 1.4 \text{ arcsec}$, and a position angle of $61 \pm 44 \text{ deg}$.

We note a high continuum emission from the center of Malin 1, which is not straightforward to explain. Some authors have noted this behavior in LINERs (Condon 1996), who quoted that LINERs are more likely to contain compact nuclear radio sources which cannot be obscured by dust than normal galaxies. Between 1 GHz and 1000 GHz, a LINER spectra is a combination of synchrotron emission, free-free emission and thermal emission from dust. However, at 100 GHz it is very difficult to disentangle the nature of the continuum emission without more continuum frequencies (Condon 1996, 1992). Other authors have proposed alternative explanations for this behavior (Yan & Blanton 2012; Singh et al. 2013).

Insisting to better understand the nature of the continuum emission, we look into the NVSS survey and FIRST survey at 1.4 GHz, and into the VLASS survey at 3 GHz, with the aim to obtain the radio spectral index for Malin 1, which in turn could give us light on the nature of the emission. Although the galaxy is only in the VLASS survey, at 3 GHz, it allow us to estimate the flux at 1.4 GHz assuming a spectral index. The flux at 3 GHz in VLASS is $390 \mu\text{Jy/beam}$, exactly at the center of Malin 1 (at 3.0 GHz, with a 2 arcsec beam). The noise in the VLASS radio image is $\sim 70 \mu\text{Jy/beam}$ (so a 5.5σ it is a VLA detection). Assuming a spectral index

of -0.7 , this would imply $665 \mu\text{Jy/beam}$ at 1.4 GHz. This is a factor of ~ 2 lower than the value estimated from extrapolating from the 3mm value using the M82 (starburst) radio SED from Condon (1992).

We then use empirical relation for star-forming galaxies between the continuum emission at 100 GHz (3 mm) and at 1.4 GHz by Heesen et al. (2014), which in turn is related to the SFR through the formula by Condon (1992), and reformulated as $\text{SFR}(M_\odot \text{ yr}^{-1}) = 0.75 \times 10^{-21} \times L_{1.4 \text{ GHz}} (\text{W Hz}^{-1})$. Using our value in luminosity units, we have $L_{1.4 \text{ GHz}} \sim 1.09 \times 10^{22} \text{ W Hz}^{-1}$. Using the Heesen et al. (2014) formula we have $\text{SFR}_{1.4 \text{ GHz}} \sim 8 M_\odot \text{ yr}^{-1}$. This value is still high compared to the $0.34 M_\odot \text{ yr}^{-1}$ from Johnston et al. (2024), suggesting contributions to the 3 mm continuum emission by other processes, like AGN activity, consistent with the LINER in the central part of Malin 1.

It is worth noting that the continuum emission was also subtracted from the visibilities using the task UVCONTSUB. This procedure was only done in the pointing centered in the nucleus of the galaxy since it is known that UVCONTSUB does not work properly when the continuum source is far from the phase center, as it is the case for the pointing centered in the disc region. The subtraction of the continuum in the uv-plane was done using the frequency range already used for IMCONTSUB and returned a set of visibilities without continuum. We then collapsed the visibilities to the same frequency range identified in the spectral cube and used to create the moment-0. Analysis in the uv-plane with UVMODELFIT returned the already mentioned values: total integrated flux of $142 \pm 21 \text{ mJy km s}^{-1}$, with a major axis of $5 \pm 0.9 \text{ arcsec}$, axis ratio of 0.67 ± 0.19 and a position angle of 34 ± 19 degree. Both estimates agree on the total flux and resolved nature of the emission.

Since the observations have marginally resolved the CO emission, we can estimate the area of a 2D Gaussian by using the following formula³:

$$\text{Area} = \frac{\pi \times \text{BMAJ} \times \text{BMIN}}{4 \ln 2}, \quad (1)$$

where BMAJ and BMIN correspond to the major and minor axis of the 2D Gaussian. The results from IMFIT return an area of $\approx 32 \text{ kpc}^2$, while the result from the uv-plane analysis returns a slightly larger area of $\approx 47 \text{ kpc}^2$. Conservatively, the emission area is estimated within $3 - 5 \times 10^7 \text{ pc}^2$, i.e. through a $1.74 - 2.25 \text{ kpc}$ radius. This represents a small fraction of the com-

³ <https://science.nrao.edu/facilities/vla/proposing/TBconv>

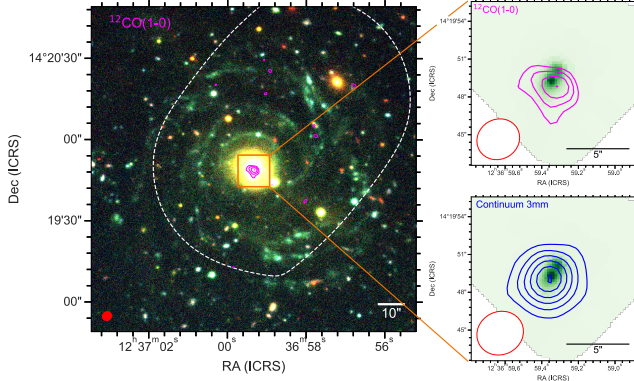


Figure 1. Continuum and $^{12}\text{CO}(1-0)$ line emission detections with ALMA band 3. The left panel shows a color optical image (u , g , i , z in blue, green, yellow, red, respectively) from Boissier et al. (2016). The inset shows the central region where continuum and line emission are significant. The red ellipse at the bottom left of each panel represents the ALMA synthesized beam size. In the main (left) panel, we show the contours of the $^{12}\text{CO}(1-0)$ velocity-integrated map superimposed to the optical image. The two panels on the right-hand side show the 3 mm continuum and $^{12}\text{CO}(1-0)$ velocity-integrated flux map contours superimposed to the $\text{H}\alpha$ emission from Junais et al. (2024). Magenta contours for the line emission over the optical and $\text{H}\alpha$ images start at 3σ and increase in steps of 1σ . For the continuum emission (bottom right panel) contours start at 3σ and increase in steps of 3σ .

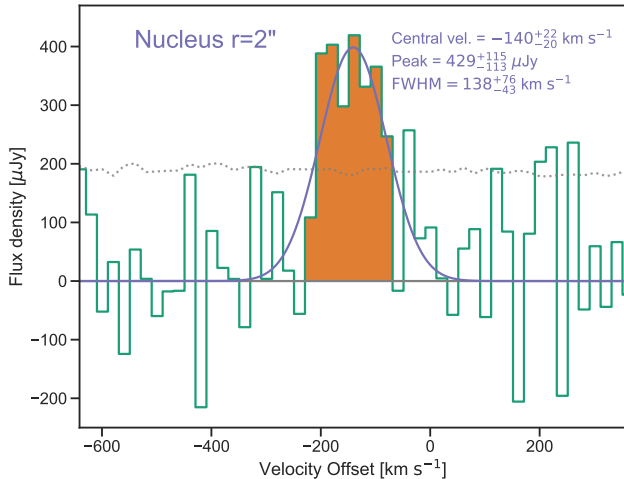


Figure 2. Line profile for the $^{12}\text{CO}(1-0)$ central detection in Malin 1. The dotted line represents the 1σ noise level, estimated as the rms measured in the cube without primary beam correction re-scaled by the square root of the ratio between the area of the aperture and the area of the synthesized beam. The line is at 6σ significance level, which is measured in the image obtained by collapsing the orange channels and comparing the peak of the signal with the rms of the background. The line is detected at a systemic velocity of $\sim -140 \text{ km s}^{-1}$ relative to the heliocentric redshift of the galaxy ($z = 0.082702$). The parameters of the best-fit Gaussian are shown in the upper right.

plete sampled area of 17,800 kpc², equivalent of a circle of radius 42 kpc. The emission is coming from $\sim 0.3\%$ of the ALMA sampled area! Given that the optical size of the galaxy is even larger, the emission is coming from a tiny part compared to the optical emission from Malin 1.

It is useful to compare the detection limit of our observations and those obtained in 2022 with the 100 m Byrd GBT telescope (Galaz et al. 2022). Although the comparison is not straightforward given the different structural principles between the GBT and ALMA (GBT a single dish and ALMA an interferometer), we can have a first approximation of the corresponding sensitivities. With the GBT, authors quote an upper limit of $\sim 90 \text{ mK km s}^{-1}$ (1σ), 7 arcsec spatial resolution, and using the line-width from the HI, of 320 km s^{-1} (Lelli et al. 2010). This corresponds to a GBT limit for the $^{12}\text{CO}(1-0)$ line in the core of Malin 1 of $\sim 60 \text{ mK km s}^{-1}$ (1σ) with a line width of $\sim 140 \text{ km s}^{-1}$, which is equivalent to $\sim 40 \text{ mJy km s}^{-1}$ (1σ), comparable to our ALMA detection limit. However, the calibration uncertainty with the GBT at 110 GHz is of order 30-50%, whereas the calibration of ALMA is much better defined, with figures of $\sim 10\%$.

3.2. Significance of detections and tentative detections

What is presented above refers to the sources detected in the nuclear region of Malin 1 both in continuum and line emission as detections based on their high signal-to-noise ratio measurement. Here we provide more details about the molecular emission search process and about robust and tentative detections.

To search for blind detections of emission lines in the spectral cubes, we used LineSeeker⁴ (González-López et al. 2019). Basically, it uses the negative side of spectral cubes as a reference for the noise and the number of

⁴ <https://github.com/jigonzal/LineSeeker>

expected false detections for a given emission line signal-to-noise ratio and width.

LineSeeker finds two high-significance emission line detections with signal-to-noise ratio values of 8.3 and 6.5. The former corresponds to a foreground galaxy with a velocity offset of $\approx -2500 \text{ km s}^{-1}$ from the Malin 1 redshift (assuming it corresponds to $^{12}\text{CO}(1-0)$), and the latter corresponds to the nuclear detection of $^{12}\text{CO}(1-0)$ in Malin 1. The search hence returns two detections of emission lines in the spectral cube set to detect $^{12}\text{CO}(1-0)$ in Malin 1, and only one is associated with it.

A second search for fainter low-significance detection of emission lines was done by applying adaptive masking of a smaller spectral cube covering $\pm 1000 \text{ km s}^{-1}$ around the central velocity of the nuclear $^{12}\text{CO}(1-0)$ in Malin 1. We use the same procedure used by [Solimano et al. \(2024\)](#) to retrieve faint and extended emissions in ALMA observations. The method consists of applying a Gaussian convolution both in the spectral and spatial axes, measuring a signal-to-noise ratio in the new convoluted cube, and then using all the voxels with $S/N \geq 3$ to create a moment-0. In this search we used a spectral Gaussian of $\sigma = 50 \text{ km s}^{-1}$ and a spatial Gaussian of $\sigma = 1.5 \text{ arcsec}$. The resulting moment-0 map is shown in Fig. 3, where three (tentative) detections (TD1, TD2, and TD3) are marked. The corresponding line emission is shown in Figure 4. These have $3 \leq S/N \leq 4$, not high enough to claim a blind detection, and thus we identify them as “tentative detections”.

Figure 3 shows that the three tentative detections do not have clear counterparts in the optical images and exhibit an offset from the main spiral arms of Malin 1. Although the lack of counterparts in the optical image would support the idea of the tentative detection being false there are documented cases where significant offsets between CO and H α emission in particular have been observed in spiral galaxies ([Egusa et al. 2004](#)). In these cases, however, the shift in radial velocity relative to the central heliocentric radial velocity of the galaxy makes the subject a little bit more complex, and will be discussed in §4.

4. DISCUSSION

In this section we discuss relevant quantities such as the CO luminosity, the molecular gas mass, the molecular gas surface density, and so on. We shall also discuss the possible nature of tentative detections presented in §3.2.

Considering a sampled area of $\sim 19 \text{ arcsec}^2$ in the central region ($\sim 47 \text{ kpc}^2$), we obtain a CO luminosity

$L'_{\text{CO}} = 4.8 \pm 0.7 \times 10^7 \text{ K km s}^{-1} \text{ pc}^{-2}$, and a total mass for the molecular gas $M_{\text{H}_2} = 2.1 \pm 0.3 \times 10^8 \text{ M}_\odot \times (\alpha_{\text{CO}}/4.4)$. We use a conversion factor α_{CO} between the integrated $^{12}\text{CO}(1-0)$ line intensity and the H $_2$ mass equal to $4.4 \text{ M}_\odot (\text{K km s}^{-1} \text{ pc}^2)^{-1}$ (see Table 1, and [Bolatto et al. 2013](#)).

With the total area of the central region estimated in 47 kpc^2 , we can compute the molecular gas mass surface density Σ_{Mol} . This returns $\Sigma_{\text{Mol}} \sim 5 \text{ M}_\odot \text{ pc}^{-2}$. This value can go down to $\Sigma_{\text{Mol}} \sim 1 \text{ M}_\odot \text{ pc}^{-2}$ if a $\alpha_{\text{CO}} = 1 \text{ M}_\odot (\text{K km s}^{-1} \text{ pc}^2)^{-1}$ is used. It is worth noting that our figures are in agreement with the corresponding value estimated by [Boissier et al. \(2016\)](#) ($\Sigma_{\text{HI+Mol}} \sim 5 \text{ M}_\odot \text{ pc}^{-2}$) based on HI density and stellar evolution synthesis model fitting.

If we consider the total or global sampled area with ALMA (the segmented region in Figure 1, $\approx 17,800 \text{ kpc}^2$), the molecular gas mass surface density Σ_{Mol} decreases to $\sim 0.01 \text{ M}_\odot \text{ pc}^{-2} \times (\alpha_{\text{CO}}/4.4)$. This figure can be considered as a lower limit, since some emission could be still undetected, with line fluxes lower than our detection threshold. At face value, this value is roughly ten times smaller than the upper limits computed by other authors ([Braine et al. 2000; Galaz et al. 2022](#)) and is perhaps one of the lowest global molecular gas surface densities computed to date from observations for a spiral galaxy.

It is also interesting to note that the star formation rate in outer spiral regions of Malin 1 as observed with the MUSE data in [Junais et al. \(2024\)](#) is much fainter than in the center. In fact, the H α surface brightness is more than three times fainter in the arms than in the center, even for the brightest regions, and up to 100 fainter for the faintest regions. In other words, if we naively assume that the CO surface brightness is dimmed the same way as H α brightness, we should not expect to have a S/N larger than ~ 2 in CO for the brightest regions in the spiral arms, even if Malin 1 lies on the K-S law.

If we scale the mass of HI ([Pickering et al. 1997; Lelli et al. 2010](#)) to the same area where the CO is detected, we obtain a molecular-to-atomic gas mass ratio close to unity. However, if we consider the total sampled area, the molecular-to-atomic gas mass ratio $M_{\text{H}_2}/M_{\text{HI}}$ decreases to $\sim 0.01/2.3 = 0.004$, where $2.3 \text{ M}_\odot \text{ pc}^{-2}$ is the atomic gas mass surface density⁵ (Σ_{HI}) for Malin 1 used by [Galaz et al. \(2022\)](#) and obtained from data of [Pickering et al. \(1997\)](#), which in turn are similar to those in [Lelli et al. \(2010\)](#). $M_{\text{H}_2}/M_{\text{HI}} = 0.004$ is an extremely low

⁵ We use here the same cosmology as in [Galaz et al. \(2022\)](#).

Table 1. Line parameters for $^{12}\text{CO}(1-0)$ detections in the center and disc regions for Malin 1. Values are obtained using Gaussian fitting. See Sections 2 and 3 for further details. Refer to Figures 1 and 3 for the corresponding identification region of emission in the galaxy.

ID	R.A.	Dec.	Central Vel.	FWHM	Flux	L'_{CO}	H_2 Mass
	2000.0	2000.0	km s^{-1}	km s^{-1}	mJy km s^{-1}	$\times 10^7 \text{ K km s}^{-1} \text{ pc}^{-2}$	$\times 10^8 \text{ M}_\odot$
(1)	(2)	(3)	(4)	(5)	(6)	(7)	(8)
Nucleus	12:36:59	+14:19:49	-140^{+22}_{-20}	138^{+76}_{-43}	142^{+21}_{-21}	$4.8^{+0.7}_{-0.7}$	$2.1^{+0.3}_{-0.3}$
TD1	12:36:57	+14:20:36	-565^{+34}_{-16}	95^{+82}_{-44}	125^{+54}_{-38}	$4.1^{+1.8}_{-1.2}$	$1.8^{+0.8}_{-0.5}$
TD2	12:37:00	+14:20:20	-99^{+33}_{-25}	103^{+96}_{-65}	75^{+35}_{-26}	$2.5^{+1.2}_{-0.8}$	$1.1^{+0.5}_{-0.4}$
TD3	12:37:00	+14:19:34	340^{+20}_{-37}	87^{+206}_{-58}	56^{+25}_{-18}	$1.9^{+0.8}_{-0.6}$	$0.8^{+0.4}_{-0.3}$

NOTE—(1) Source ID. (2) RA. (3) Dec. (4) Heliocentric central velocity with respect to $z = 0.082702$. (5) FWHM of a Gaussian fit to the emission line. (6) Integrated flux of the emission line in mJy km s^{-1} . (7) CO Luminosity. (8) Molecular mass assuming $\alpha_{\text{CO}} = 4.4 \text{ M}_\odot (\text{K km s}^{-1} \text{ pc}^2)^{-1}$.

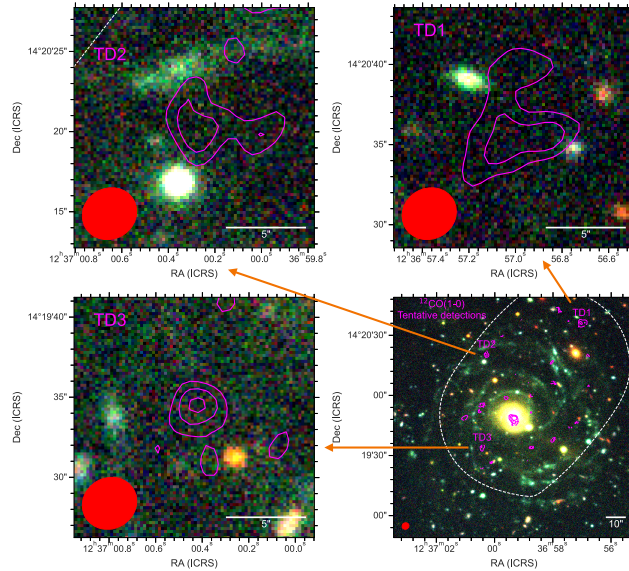


Figure 3. Disc location of the three tentative detections. We show here detections with $3 \leq \text{S/N} \leq 4$ of the peak of the collapsed lines, as indicated in the bottom right panel, where they are superimposed over a composite optical image (Boissier et al. 2016). Line detections denoted as TD1, TD2, and TD3 are amplified in the other panels. The corresponding line emission profiles are shown in Figure 4. Other fainter emissions in the disc have S/N smaller than 2, and are not considered, but also shown in this Figure.

value, and it is a clear indication of the scarcity of the molecular gas in Malin 1 along its enormous extension.

The obtained molecular gas mass surface density Σ_{Mol} can be used to better understand the star-forming properties of Malin 1. These properties can be compared to those computed for other galaxies. In particular, it is worth comparing the obtained values here with those computed in star-forming spiral galaxies where the molecular gas has been studied, along with the star formation rate surface density of these galaxies. Figure 5 shows the position of Malin 1 in the so-called

Kennicutt-Schmidt diagram (Kennicutt 1998; Krumholz et al. 2009), but in terms of the molecular gas surface density Σ_{Mol} instead of the typical atomic gas surface density Σ_{HI} , compared to the values obtained for the sample of galaxies detected within the PHANGS-ALMA survey (Sun et al. 2023).

Considering the total surveyed area, it is clear that Malin 1 lies at the bottom end of the star-forming sequence but with very short molecular gas depletion times (green star in Figure 5). On the other hand, when only the central region is considered to compute the area

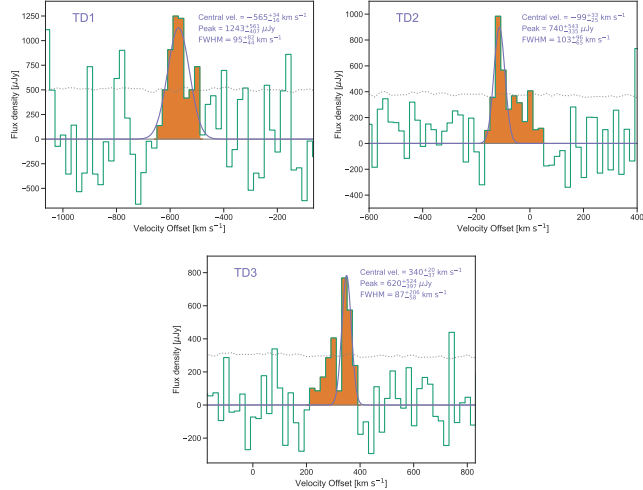


Figure 4. $^{12}\text{CO}(1-0)$ line profiles of tentative detections. These correspond to the emissions shown in Figure 3. These detections have $3 \leq \text{S/N} \leq 4$. Some features of the line fitting are shown in the upper right of each line profile.

where also the molecular gas surface density is much larger, the star formation rate surface density increases to the level of normal galaxies (magenta star in Figure 5). In other words, the central region of Malin 1 seems to convert molecular gas into stars not too differently from what is observed in normal spiral galaxies. From one side this supports what has been suggested earlier: the central part of Malin 1 behaves like an individual spiral galaxy, regardless of what is happening far outside in its diffuse disc (Barth 2007). For reference, recall that in optical bands the central part of Malin 1 has a similar size of the Milky Way (MW), i.e. $\simeq 30$ kpc. However, the fact that for more than 30 years CO detections have failed by different authors and instruments tells us that, still, the star-formation rate surface density in the very center of Malin 1 is not high ($\sim 10^{-3} M_{\odot} \text{ yr}^{-1} \text{ kpc}^{-2}$), as Figure 5 shows.

Given the outstanding spatial resolution of MUSE at the VLT and ALMA, allowing to combine H α data from the first instrument with CO data from the second one, we are able to trace the star formation rate surface density as a function of the molecular gas density along different radii in the central part of Malin 1, as the colored line shows in Figure 5. We see that in spite of the relatively narrow range of space within the center of Malin 1 (~ 20 kpc), the star formation rate surface density drops from $\sim 2 \times 10^{-3} \text{ M}_\odot \text{ yr}^{-1} \text{ kpc}^{-2}$ to $\sim 4 \times 10^{-5} \text{ M}_\odot \text{ yr}^{-1} \text{ kpc}^{-2}$, with molecular gas mass densities varying from $\sim 2 \text{ M}_\odot \text{ pc}^{-2}$ to $\sim 0.8 \text{ M}_\odot \text{ pc}^{-2}$, respectively.

In Figure 5 we also show the position of gLSBGs UGC 6614 and Malin 2, two of the few gLSBGs with measured CO emission (Das et al. 2006, 2010; Wyder et al. 2009).

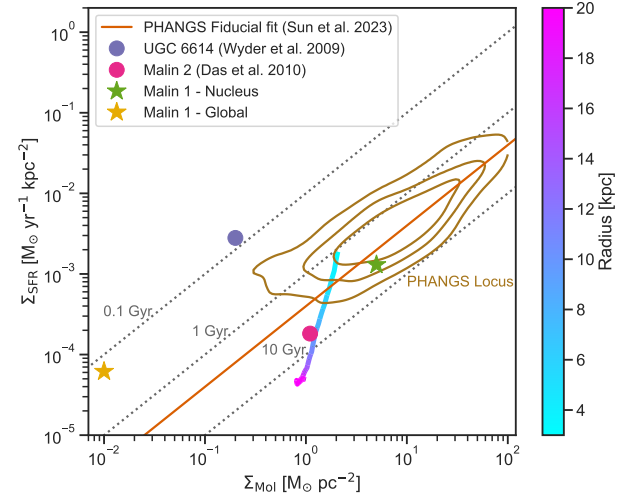


Figure 5. Kennicutt–Schmidt diagram for the molecular gas in Malin 1 (Kennicutt 1998; Krumholz et al. 2009). This plot shows the range of stellar formation surface density as a function of the molecular gas surface density for different area coverage and detections. The star formation surface density Σ_{SFR} in the very center (magenta star) is $\sim 2 \times 10^{-3} \text{ M}_\odot \text{ yr}^{-1} \text{ kpc}^{-2}$ and has a molecular gas mass surface density $\Sigma_{\text{Mol}} \sim 5 \text{ M}_\odot \text{ pc}^{-2}$, compared to the global Σ_{SFR} (i.e. considering the total surveyed area; green star) of $\sim 6 \times 10^{-5} \text{ M}_\odot \text{ yr}^{-1} \text{ kpc}^{-2}$ with a corresponding molecular gas surface density of $\sim 0.01 \text{ M}_\odot \text{ pc}^{-2}$. The thin dotted lines represent linear relations with constant molecular gas depletion times of 0.1, 1, and 10 Gyr. The density contours (40%–80%–95% levels from inside to outside contours) represent the distributions of all 1.5 kpc scale regions with $> 3\sigma$ detections for both Σ_{Mol} and Σ_{SFR} for galaxies studied in the PHANGS-ALMA sample (Sun et al. 2023). The colored-gradient trace represents the 5σ upper limit molecular gas surface density combined with the corresponding star formation rate surface density measured with MUSE (Junais et al. 2024). The different radii for the estimates are shown in the color bar on the right. We show also the position of the gLSBGS UGC 6614 and Malin 2 (Das et al. 2006, 2010; Wyder et al. 2009). See Section 4 for details.

For UGC 6614, Σ_{H_2} represents the global molecular gas mass surface density, i.e. the quantity obtained considering the total surveyed area. For Malin 2, we plot the molecular gas mass surface density obtained considering only the region where the emission is detected (as our case for Malin 1 with the colored bar). For the global emission, UGC 6614 still has a global $\Sigma_{\text{Mol}} \sim 0.2 \text{ M}_\odot \text{ pc}^{-2}$, a value 20 times larger to the one we obtain here for Malin 1 (green star). The case of Malin 2 seems not too different than that for Malin 1, although Malin 2 is half of the size of Malin 1.

Now we discuss the possible nature of the $^{12}\text{CO}(1-0)$ emission from regions TD1, TD2, and TD3 (what we dubbed “tentative detections”). Figure 4 shows the

corresponding line profiles for our tentative detections, which in addition show for TD1 and TD3 large radial velocity shifts relative to the systemic velocity of Malin 1 (see also Table 1, that presents some properties of the $^{12}\text{CO}(1-0)$ line detections). Lelli et al. (2010) improved the HI velocity field from Pickering et al. (1997) and concluded that there is up to $\pm 200 \text{ km s}^{-1}$ difference between systemic velocity of Malin 1 and the northern (positive velocities) and southern (negative velocities) extreme sides of the disc in Malin 1, compatible with the observations performed in ionized gas with MUSE (Johnston et al. 2024), which also confirms the result of Junais et al. (2020) that high velocities are reached close to the center. This suggests that TD1 and TD3 are exceeding the HI radial velocity by more than $\sim 400 \text{ km s}^{-1}$, making therefore difficult to associate these two emissions to Malin 1, and making these emissions uncertain from the point of view of their actual nature. Note that Pickering et al. (1997) and Lelli et al. (2010) also identify a potential HI warp at those distances (PA variations), further revealing the complexity of this large disc structure.

The case of TD2 is more favorable to belong to Malin 1 disc, especially when comparing the velocity difference with the central detection of $\sim +40 \text{ km s}^{-1}$ with the expected velocity shift that is close to $+100 \text{ km s}^{-1}$ in that region. In any case, the question still stands. If TD1 and TD3 emissions do not come from Malin 1, where do they come from? Although this issue escapes the scope of this paper, we include these results here. An element that could shed some light on this issue is the possible association of these emissions to high-velocity clouds in Malin 1. Such clouds are not necessarily associated with optical counterparts and have been observed in the Local Group and in the Milky Way, and are the subject of discussions (Bregman 1980; Wakker & van Woerden 1997; Blitz et al. 1999). Furthermore, our preliminary semi-analytic orbital calculations⁶ suggest that TD2 and TD3 could have orbits bound to the Malin 1 system, while TD1 is probably associated with an external source.

An interesting possibility for Malin 1 is the presence of CO-dark molecular gas (DMG), which refers to molecular gas not traced by CO emission. This gas has been identified in the solar neighborhood and recently in the Milky Way, 13 kpc from the galactic center (Luo et al. 2024). This raises the potential that Malin 1 is replenished with DMG, making CO a poor tracer. Such a scenario is plausible given that the visual extinction, H_2

density, and molecular fraction of DMG are similar to those in nearby diffuse molecular clouds. Ramambason et al. (2024) also explore stellar formation in low-metallicity galaxies and highlight the role of DMG. They conclude that low-metallicity galaxies with high clumpiness parameters may exhibit α_{CO} values comparable to the Galactic value, even at low metallicity. While Malin 1 is not significantly low in metallicity, it may possess a turbulent ISM (indicated by velocity dispersions) and a high conversion factor, potentially eliminating the need to invoke DMG. However, confirming clumpiness requires higher resolution observations.

This specific topic, together with other secure detections associated to other sources in the field, will be investigated in further detail, in a forthcoming paper.

5. SUMMARY AND CONCLUSIONS

In this work we have finally detected CO in the iconic gLSBG Malin 1. We detected continuum and $^{12}\text{CO}(1-0)$ emissions in the center of Malin 1, in a position which is consistent with findings and analysis of $\text{H}\alpha$ emission recently obtained (Junais et al. 2024; Johnston et al. 2024). The total central continuum flux density is $107 \pm 12 \mu\text{Jy}$, and the velocity-integrated flux density for the $^{12}\text{CO}(1-0)$ line is $143 \pm 41 \text{ mJy km s}^{-1}$. This yields a CO luminosity $L'_{\text{CO}} = 4.8 \pm 0.7 \times 10^7 \text{ K km s}^{-1} \text{ pc}^{-2}$. The total estimated molecular mass is $\sim 2.1 \pm 0.3 \times 10^8 \text{ M}_\odot \times (\alpha_{\text{CO}}/4.4)$ and the central molecular gas mass surface density is $\Sigma_{\text{Mol}} \sim 3-5 \text{ M}_\odot \text{ pc}^{-2}$. However, when considering the total sampled area, Σ_{Mol} is reduced to $\sim 0.01 \text{ M}_\odot \text{ pc}^{-2}$. With these figures, the molecular-to-atomic gas mass ratio is ~ 0.04 for Malin 1.

We also report on three tentative detections in the disc. Because of large velocity shifts relative to the systemic velocity of Malin 1, only one of these detections seems to be robust and can be associated to Malin 1.

In this work we provide solid evidence of the existence of molecular gas in the largest spiral galaxy observed so far. The goal to detect CO in Malin 1 has now been reached. Results presented here show not only that Malin 1 has a very low global star formation rate surface density and extremely low global molecular gas surface density, as former upper limits anticipated (Braine et al. 2000; Galaz et al. 2022), but also that the stellar formation is sparse and at the same time spotty, along its vast physical extension. This is consistent with conclusions of other authors (Boissier et al. 2016; Schombert & McGaugh 2014), who claim an intermittent star-formation history, supported by colors of individual regions. Nevertheless, our results, along with those obtained recently (Junais et al. 2024), suggest that galaxies as large and diffuse as Malin 1 are forming stars in a significant num-

⁶ Bustos-Espinoza et al. (2025, in preparation).

ber of spots along their huge discs, in spite of their extremely low global molecular gas surface densities compared to other galaxies. The emerging picture is that these star-forming spots seem quite isolated, with star-forming processes that seem to challenge typical scales observed in HSB spiral galaxies. A more profound understanding of the actual conversion of molecular gas into stars taking place at these gas densities needs more precise and higher resolution mm observations. This includes an actual determination of the conversion factor at these extremely low molecular gas mass surface densities and likely different ISM temperatures. The exact physical processes that explain the distribution of the molecular gas in Malin1 is now open and hopefully better constrained for future works.

We would like to thank the anonymous referee for their insightful suggestions, which improved the quality and clarity of this paper. G.G., V.G., T.P., R.B., K.J., and E.J.J. gratefully acknowledge support by the ANID BASAL projects ACE210002 and FB210003. G.G. acknowledges the support of Pontificia Universidad Católica de Chile through a sabbatical grant, as well as the European Southern Observatory (ESO) for support during the completion of this work. E.J.J. acknowledges support from FONDECYT Iniciación en Investigación 2020 Project 11200263. J. is funded by the European Union (MSCA EDUCADO, GA 101119830 and WIDERA ExGal-Twin, GA 101158446). This paper makes use of the following ALMA data: ADS/JAO.ALMA#2023.1.01105.S. ALMA is a partnership of ESO (representing its member states), NSF (USA) and NINS (Japan), together with NRC (Canada), NSTC and ASIAA (Taiwan), and KASI (Republic of Korea), in co-operation with the Republic of Chile. The Joint ALMA Observatory (JAO) is operated by ESO, AUI/NRAO and NAOJ. The National Radio Astronomy Observatory (NRAO) is a facility of the National Science Foundation operated under cooperative agreement by Associated Universities, Inc. This research has made use of the Astrophysics Data System, funded by NASA under Cooperative Agreement 80NSSC21M00561. This research has made use of the Sloan Digital Sky Survey (SDSS) data. Funding for the SDSS has been provided by the Alfred P. Sloan Foundation, the Participating Institutions, the National Science Foundation, the U.S. Department of Energy, the National Aeronautics and Space Administration, the Japanese Monbukagakusho, the Max Planck Society, and the Higher Education Funding Council for England. The SDSS Web Site is <http://www.sdss.org/>. The SDSS is managed by the Astrophysical Research Consortium for the Participating Institutions.

REFERENCES

Barth, A. J. 2007, AJ, 133, 1085, doi: [10.1086/511180](https://doi.org/10.1086/511180)

Blitz, L., Spergel, D. N., Teuben, P. J., Hartmann, D., & Burton, W. B. 1999, ApJ, 514, 818, doi: [10.1086/306963](https://doi.org/10.1086/306963)

Boissier, S., Boselli, A., Ferrarese, L., et al. 2016, A&A, 593, A126, doi: [10.1051/0004-6361/201629226](https://doi.org/10.1051/0004-6361/201629226)

Bolatto, A. D., Wolfire, M., & Leroy, A. K. 2013, ARA&A, 51, 207, doi: [10.1146/annurev-astro-082812-140944](https://doi.org/10.1146/annurev-astro-082812-140944)

Bothun, G. D., Impey, C. D., Malin, D. F., & Mould, J. R. 1987, AJ, 94, 23, doi: [10.1086/114443](https://doi.org/10.1086/114443)

Braine, J., Herpin, F., & Radford, S. J. E. 2000, A&A, 358, 494

Bregman, J. N. 1980, ApJ, 236, 577, doi: [10.1086/157776](https://doi.org/10.1086/157776)

Bustos-Espinoza, R., et al. 2025, in preparation

Condon, J. J. 1992, ARA&A, 30, 575, doi: [10.1146/annurev.aa.30.090192.003043](https://doi.org/10.1146/annurev.aa.30.090192.003043)

Condon, J. J. 1996, in Astronomical Society of the Pacific Conference Series, Vol. 103, The Physics of Liners in View of Recent Observations, ed. M. Eracleous, A. Koratkar, C. Leitherer, & L. Ho, 132

Dalcanton, J. J., Spergel, D. N., Gunn, J. E., Schmidt, M., & Schneider, D. P. 1997, AJ, 114, 635, doi: [10.1086/118499](https://doi.org/10.1086/118499)

Das, M., Boone, F., & Viallefond, F. 2010, A&A, 523, A63, doi: [10.1051/0004-6361/200913794](https://doi.org/10.1051/0004-6361/200913794)

Das, M., O’Neil, K., Vogel, S. N., & McGaugh, S. 2006, ApJ, 651, 853, doi: [10.1086/507410](https://doi.org/10.1086/507410)

de Blok, W. J. G., & McGaugh, S. S. 1997, MNRAS, 290, 533, doi: [10.1093/mnras/290.3.533](https://doi.org/10.1093/mnras/290.3.533)

Disney, M. J. 1976, Nature, 263, 573, doi: [10.1038/263573a0](https://doi.org/10.1038/263573a0)

Egusa, F., Sofue, Y., & Nakanishi, H. 2004, PASJ, 56, L45, doi: [10.1093/pasj/56.6.L45](https://doi.org/10.1093/pasj/56.6.L45)

Freeman, K. C. 1970, ApJ, 160, 811, doi: [10.1086/150474](https://doi.org/10.1086/150474)

Galaz, G., Milovic, C., Suc, V., et al. 2015, ApJL, 815, L29, doi: [10.1088/2041-8205/815/2/L29](https://doi.org/10.1088/2041-8205/815/2/L29)

Galaz, G., Frayer, D. T., Blaña, M., et al. 2022, ApJL, 940, L37, doi: [10.3847/2041-8213/aca146](https://doi.org/10.3847/2041-8213/aca146)

Gerritsen, J. P. E., & de Blok, W. J. G. 1999, A&A, 342, 655, doi: [10.48550/arXiv.astro-ph/9810096](https://doi.org/10.48550/arXiv.astro-ph/9810096)

González-López, J., Decarli, R., Pavesi, R., et al. 2019, ApJ, 882, 139, doi: [10.3847/1538-4357/ab3105](https://doi.org/10.3847/1538-4357/ab3105)

Heesen, V., Brinks, E., Leroy, A. K., et al. 2014, AJ, 147, 103, doi: [10.1088/0004-6256/147/5/103](https://doi.org/10.1088/0004-6256/147/5/103)

Impey, C., & Bothun, G. 1989, ApJ, 341, 89, doi: [10.1086/167474](https://doi.org/10.1086/167474)

Impey, C. D., Sprayberry, D., Irwin, M. J., & Bothun, G. D. 1996, ApJS, 105, 209, doi: [10.1086/192313](https://doi.org/10.1086/192313)

Johnston, E. J., Galaz, G., Blaña, M., et al. 2024, A&A, 686, A247, doi: [10.1051/0004-6361/202348587](https://doi.org/10.1051/0004-6361/202348587)

Junais, Boissier, S., Epinat, B., et al. 2020, A&A, 637, A21, doi: [10.1051/0004-6361/201937330](https://doi.org/10.1051/0004-6361/201937330)

Junais, Weilbacher, P. M., Epinat, B., et al. 2024, A&A, 681, A100, doi: [10.1051/0004-6361/202347669](https://doi.org/10.1051/0004-6361/202347669)

Kennicutt, Robert C., J. 1998, ApJ, 498, 541, doi: [10.1086/305588](https://doi.org/10.1086/305588)

Krumholz, M. R., McKee, C. F., & Tumlinson, J. 2009, ApJ, 699, 850, doi: [10.1088/0004-637X/699/1/850](https://doi.org/10.1088/0004-637X/699/1/850)

Lelli, F., Fraternali, F., & Sancisi, R. 2010, A&A, 516, A11, doi: [10.1051/0004-6361/200913808](https://doi.org/10.1051/0004-6361/200913808)

Luo, G., Li, D., Zhang, Z.-Y., et al. 2024, A&A, 685, L12, doi: [10.1051/0004-6361/202450067](https://doi.org/10.1051/0004-6361/202450067)

Maddox, S. J., Sutherland, W. J., Efstathiou, G., & Loveday, J. 1990, MNRAS, 243, 692

Martin, G., Kaviraj, S., Laigle, C., et al. 2019, MNRAS, 485, 796, doi: [10.1093/mnras/stz356](https://doi.org/10.1093/mnras/stz356)

O’Neil, K., & Bothun, G. 2000, ApJ, 529, 811, doi: [10.1086/308322](https://doi.org/10.1086/308322)

O’Neil, K., Hofner, P., & Schinnerer, E. 2000, ApJL, 545, L99, doi: [10.1086/317893](https://doi.org/10.1086/317893)

O’Neil, K., Schneider, S. E., van Driel, W., et al. 2023, AJ, 165, 263, doi: [10.3847/1538-3881/acd345](https://doi.org/10.3847/1538-3881/acd345)

Pickering, T. E., Impey, C. D., van Gorkom, J. H., & Bothun, G. D. 1997, AJ, 114, 1858, doi: [10.1086/118611](https://doi.org/10.1086/118611)

Radford, S. J. E. 1992, A&A, 262, 13

Ramambason, L., Lebouteiller, V., Madden, S. C., et al. 2024, A&A, 681, A14, doi: [10.1051/0004-6361/202347280](https://doi.org/10.1051/0004-6361/202347280)

Reshetnikov, V. P., Moiseev, A. V., & Sotnikova, N. Y. 2010, MNRAS, 406, L90, doi: [10.1111/j.1745-3933.2010.00888.x](https://doi.org/10.1111/j.1745-3933.2010.00888.x)

Saha, K., Dhiwar, S., Barway, S., Narayan, C., & Tandon, S. 2021, Journal of Astrophysics and Astronomy, 42, 59, doi: [10.1007/s12036-021-09715-5](https://doi.org/10.1007/s12036-021-09715-5)

Schombert, J., & McGaugh, S. 2014, PASA, 31, e036, doi: [10.1017/pasa.2014.32](https://doi.org/10.1017/pasa.2014.32)

Singh, R., van de Ven, G., Jahnke, K., et al. 2013, A&A, 558, A43, doi: [10.1051/0004-6361/201322062](https://doi.org/10.1051/0004-6361/201322062)

Solimano, M., González-López, J., Aravena, M., et al. 2024, arXiv e-prints, arXiv:2401.04919, doi: [10.48550/arXiv.2401.04919](https://doi.org/10.48550/arXiv.2401.04919)

Sun, J., Leroy, A. K., Ostriker, E. C., et al. 2023, ApJL, 945, L19, doi: [10.3847/2041-8213/acbd9c](https://doi.org/10.3847/2041-8213/acbd9c)

van der Hulst, J. M., Skillman, E. D., Smith, T. R., et al. 1993, AJ, 106, 548, doi: [10.1086/116660](https://doi.org/10.1086/116660)

Wakker, B. P., & van Woerden, H. 1997, ARA&A, 35, 217, doi: [10.1146/annurev.astro.35.1.217](https://doi.org/10.1146/annurev.astro.35.1.217)

Wyder, T. K., Martin, D. C., Barlow, T. A., et al. 2009, ApJ, 696, 1834, doi: [10.1088/0004-637X/696/2/1834](https://doi.org/10.1088/0004-637X/696/2/1834)

Yan, R., & Blanton, M. R. 2012, ApJ, 747, 61, doi: [10.1088/0004-637X/747/1/61](https://doi.org/10.1088/0004-637X/747/1/61)